Journal of Power Sources 252 (2014) 252–263

Contents lists available at ScienceDirect

Journal of Power Sources

journal homepage: www.elsevier.com/locate/jpowsour

Morphologically architectured spray pyrolyzed lanthanum ferrite-based cathodes—A phenomenal enhancement in solid oxide fuel cell performance

Jayanta Mukhopadhyay, Rajendra Nath Basu*

Fuel Cell and Battery Division, CSIR – Central Glass and Ceramic Research Institute, Kolkata 700 032, India

HIGHLIGHTS

- Nanocrystalline $La_{1-x}Sr_xCo_{1-y}Fe_yO_{3-\delta}$ cathodes synthesized by novel spray pyrolysis.
- Tailored particulate morphology by in-situ homomolecular seeding during pyrolysis.
- Polarization lowered to 0.032 Ω cm^2 at 800 °C using morphologically tailored cathode.
- High exchange current density (0.7 A cm^{-2}, 800 °C) found for oxygen reduction reaction.
- Optimized LSCF exhibits current density ~4.0 A cm^{-2} (0.7 V, 800 °C) with H_2 and air.

ARTICLE INFO

Article history:
Received 23 October 2013
Received in revised form
29 November 2013
Accepted 30 November 2013
Available online 10 December 2013

Keywords:
Spray pyrolysis
Solid oxide fuel cell
Morphologically architectured cathode
Interfacial polarization
High current density
Electrochemical performance

ABSTRACT

Nanocrystalline single phase $La_{1-x}Sr_xCo_{1-y}Fe_yO_{3-\delta}$ [LSCF] ($0 < x \leq 0.5$, $y = 0.2, 0.8$) based cathodes (crystallite size 30–50 nm) are synthesized by two fluid spray-pyrolysis (SP) for solid oxide fuel cell (SOFC) application. The particulate sizes of the synthesized cathodes are found to be in the range of 100–200 nm. Particulate morphology of highest conducting cathode (~1500 S cm^{-1}) is tailored using homomolecular seeding agent of precalcined pyrolyzed ashes. Interfacial polarizations of the such SP synthesized screen printed cathodes onto gadolinium doped ceria (CGO) based electrolyte are found to be much lower (0.032–0.16 Ω cm^2 at 800 °C–500 °C) with highest exchange current density (~722 mA cm^{-2} at 800 °C) for oxygen reduction reaction. Enhanced current density of 4.0 A cm^{-2} (0.7 V, 800 °C) is obtained for SOFC button cells using optimized LSCF cathode with hydrogen as fuel and air as oxidant. LSCF cathodes synthesized by spray pyrolysis using homomolecular seeding exhibit interconnected mesoporosity having primary nano-particulates embedded within. Endurance test of button cells till 500 h results low degradation viz. 3.8% and 8.9% 1000 h^{-1} with electronic loads of 0.5 A cm^{-2} and 1.0 A cm^{-2} respectively. High performances of such cells are clinically correlated with SP processing conditions and particulate morphology of cathode powders.

1. Introduction

In search for efficient energy generation, solid oxide fuel cell (SOFC) technology has gained considerable attention due to their ability to convert chemical energy directly into electrical energy with high efficiency (>50%), multi-fuel capability and environmental benign nature of power generation. High operating temperature (800–1000 °C) required for SOFC application place heavy demands on the material components. Such a high temperature of operation also accelerates fuel cell degradation. To increase the lifetime and to reduce system costs, the reduction of operating temperature of SOFC is found to be essential. Chemical and thermal stability of the cell components with proper interfacial bonding and interaction with the oxidant and reductant species at lower operating temperatures are the key factors governing the net electrochemical performance of single cell which dictates the final efficiency [1–4]. The performance of conventional $La_{1-x}Sr_xMnO_{3-\delta}$ (LSM) which acts as a cathode catalyst at or above 800 °C for anode-supported SOFC is found to be unsatisfactory at lower temperature than 800 °C due to sluggish oxygen reduction reaction (ORR) kinetics that limits the application in intermediate temperature SOFCs [5,6]. Thermodynamic and experimental studies showed that mixed ionic electronic conductor (MIEC) based materials could

* Corresponding author. Tel.: +91 33 24292951; fax: +91 33 24730957.
E-mail addresses: rajenbasu54@gmail.com, rnbasu@cgcri.res.in (R.N. Basu).

0378-7753/$ – see front matter © 2013 Elsevier B.V. All rights reserved.
http://dx.doi.org/10.1016/j.jpowsour.2013.11.116

be a potential alternative to enhance the cathode performance in the lower temperature range of operation. Owing to the presence of both high electronic and reasonable ionic conductivity along with high catalytic activity, it is reported that ORR of the cathode can be significantly enhanced [7–10]. Several new compositions with MIEC nature have been reported as a promising SOFC cathode that can extend the active electrochemical reaction sites from traditional triple phase boundaries (TPBs) at the solid electrolyte/electronic-conductor electrode interface to the entire MIEC/gas interface [2–4,11–17]. Recently, lowering of the operating temperature of SOFC at around 650 °C along with high quality performance involving MIEC class of cathode materials are reported by many group of researchers [18,19]. $La_{1-x}Sr_xCo_{1-y}Fe_yO_{3-\delta}$ (LSCF), one of the most promising class of perovskite cathodes, have attracted considerable attention due to its MIEC nature, higher catalytic activity for oxygen reduction reaction and better degree of stability in the lower range of intermediate temperature SOFC i.e. IT-SOFC (~700 °C). Therefore, LSCF is found to be effective for electrically driven ceramic oxygen generators (COG) and dense membranes for pressure driven oxygen separators [20–22]. It is worth to mention that not only the composition but also particle size and morphology are important for electrochemical performance enhancement of such perovskite based meso and microporous MIEC cathode materials. Different powder preparation routes for LSCF-based materials are reported in the literature. Mori et al. [23] prepared $LaCoO_3$ by conventional solid-state reaction method followed by calcination at 1000 °C for 12 h, whereas, similarly Sase et al. [24] employed the co-precipitation technique. Several other conventional and advanced techniques such as combustion synthesis, polymerizable complex method, sputtering lithography, and etching etc. have been attempted for synthesizing such MIEC cathode in the form of bulk powders or thin films [25–27]. Nanometer scaled and nanoporous $La_{0.6}Sr_{0.4}CoO_{3-\delta}$ (LSC) exhibiting enhanced oxygen surface-exchange properties synthesized by metal-organic precursors as thin film cathodes of about 200 nm thickness and their details characterizations were reported by Hayd et al. [28,29]. Fu et al. [30] reported the as-deposited amorphous LSCF films from perovskite crystals after calcination of 750 °C for 2 h by electrostatic spray deposition. Almost similar approach but with air pressurized spray pyrolysis technique with lower calcination temperature has been reported by Beckel et al. [31]. Spray pyrolysis (SP) is one of the most effective techniques to synthesize a variety of such multicomponent ceramic materials in a semi-continuous mode of operation. SP can not only generate highly proactive nanocrystalline materials but also enables controlling of particulate morphology by proper tuning of the process parameters [32]. In addition, SP offers specific advantages, viz. higher purity of the produced powders, a better uniformity in chemical composition, a narrower size distribution, better regularity in shape and synthesis of multicomponent materials [32–35]. The major steps responsible for the generation of either dense or hollow particulates by SP depend on the effective droplet generation by atomization technique. This is followed by their transport, solvent evaporation and concomitant solute precipitation with the thermolysis of precipitated particles at higher temperatures to form micro/meso-porous particles. Depending upon the synthesis and processing techniques, nanocrystalline nature of the LSCF-based cathode helps in enhancing the single cell performance. Some important research findings in regard to such MIEC system are also reported in our earlier work [36,37]. In the present investigation, various compositions of nanocrystalline lanthanum ferrite-based cathodes ($La_{1-x}Sr_xCo_{1-y}Fe_yO_{3-\delta}$ where, $0 < x \leq 0.5$, $y = 0.2$ and 0.8) are synthesized by low temperature (~450 °C) two fluid aerosol SP technique. The basic endeavor of the present research is based on the tailoring of spray parameter which governs the microstructure of newly formed particulates. Spray parameters viz. atomization pressure, feed rate and precursor properties are optimized to generate nanocrystalline LSCF cathodes with necessary in-built meso and micro pores. Thermal and electrical properties are attempted to correlate with composition and synthesis parameters of the cathodes. Electrochemical impedance spectroscopic (EIS) studies of such spray pyrolyzed cathodes are carried out for measuring the interfacial resistances with doped ceria (CGO)-based electrolyte. Particulate morphology of the synthesized LSCF cathodes is also tailored with the addition of the precalcined ashes as the seeding agent for substantial growth. Oxygen reduction reaction (ORR) kinetics of the various cathodes synthesized using such SP technique are also calculated from EIS. Electrochemical performances and endurance test upto 500 h of the anode-supported single cells (Ni–YSZ/YSZ/CGO/LSCF) are carried out with the optimized cathodes using gadolinium doped ceria (CGO)-based interlayer, prepared by combustion synthesis [37]. Properties of the single cells are correlated with cathode microstructures which in turn is highly dependent on various synthesizing conditions of SP technique.

2. Experimental

2.1. Synthesis of LSCF cathode powders by spray pyrolysis technique and their characterizations

The cathode compositions which were studied under the present investigation are given in Table 1 along with their precursor solution concentration. For synthesis of such LSCF based cathodes by SP technique, a precursor salt solution consisting of stoichiometric amount of lanthanum (III) nitrate hexahydrate (Sisco Research Laboratory, India, 99.9%) and strontium (II) nitrate (E Merck India Limited, 98%) were mixed in a beaker. Salts of iron (III) nitrate nonahydrate (Acros Organics, >99%) and cobalt (II) nitrate hexahydrate (Merck India Limited, 97%) were added to the aqueous solution as the source of iron and cobalt respectively. The solution was mixed in such a proportion that the overall concentration of the metal ions becomes 0.25 M. This mixed solution was heated on a magnetic stirrer with continuous stirring and allowed to evaporate. Stoichiometric amount of fuel like glycine (Acros Organics, >99%) was added to precursor metal salt solution at a definite fuel to nitrate ratio of 0.75:1. Based on the characteristic of thermal decomposition of glycine–metal complexes, citric acid monohydrate (Merck Limited, 99.5%) was also added to the fuel and the ratio of glycine and citric acid was kept 1:1. The components were mixed as described above but polymerization was arrested at an intermediate stage to control the viscosity of the solution suitable for spraying. Such a precursor solution was atomized through a tiny bore two fluid nozzle into the hot chamber of an indigenously designed spray pyrolyzer unit. While the bore diameter of the nozzle was kept constant at 0.7 mm, the flow rate of the atomized precursor solution was kept constant at 20 ml min^{-1} and the

Table 1
Cathode compositions and their corresponding sample IDs.

Cathode composition	Sample ID
$La_{0.8}Sr_{0.2}Co_{0.8}Fe_{0.2}O_{3-\delta}$	LSCF-1
$La_{0.8}Sr_{0.2}Co_{0.2}Fe_{0.8}O_{3-\delta}$	LSCF-2
$La_{0.65}Sr_{0.3}Co_{0.8}Fe_{0.2}O_{3-\delta}$	LSCF-3
$La_{0.65}Sr_{0.3}Co_{0.2}Fe_{0.8}O_{3-\delta}$	LSCF-4
$La_{0.5}Sr_{0.5}Co_{0.8}Fe_{0.2}O_{3-\delta}$	LSCF-5
$La_{0.5}Sr_{0.5}Co_{0.2}Fe_{0.8}O_{3-\delta}$	LSCF-6
$La_{0.5}Sr_{0.5}Co_{0.8}Fe_{0.2}O_{3-\delta}$ + 25% (w/w) solid loading of precalcined ashes	LSCF-5A

compressed air (atomization air) pressure was maintained at 140 kPa. Atomization of the precursor solutions was carried out in the reaction chamber temperature at ~450 °C (gas inlet temperature sensor) during spraying. The atomization pressure is calculated to be 1.36 MPa with the volumetric flow rates of the solution and compressed air pressure as mentioned above. The exhaust gases were scrubbed out using a conventional wet scrubber. The synthesized powders were calcined at a temperature of 750 °C for 4 h. The schematic of the spray pyrolysis process employed in the present investigation is given in Fig. 1. In-situ growth of the pyrolyzed nanocrystalline cathode was practised by adding the spray pyrolyzed precalcined ashes as the seeding agent in the precursor solution. In such cases, 25 wt. % solid loading was employed to the precursor solution and the batch formulation for the same is also tabulated in Table 1. Under the present investigation, the effect of such particle growth is reported for the highest conducting cathode materials. In order to optimize the thermal decomposition of the precursor solution, thermogravimetric analysis (TGA) of the complex gels prepared with the mixed and single fuels were carried out separately by a Shimadzu TA-50 Thermal Analyzer from room temperature to 800 °C in air at a heating rate of 10 °C min^{-1}. Phase identification of the calcined LSCF powders was confirmed by X-ray powder diffraction (XRD) at a scan rate of 2° min^{-1} in the range of 10°–80° on a X-ray diffractometer (Philips X'pert, PANalytical, Netherlands) with Cu-Kα radiation. Rietveld refinement of the diffraction data was carried out by PANalytical X'Pert High Score software using a pseudovoight function. To study the microstructure of SP nanocrystalline cathode powders synthesized under various processing conditions, field emission scanning electron micrographs (FESEM, Gemini Supra 35, Zeiss) were carried out. The coefficient of thermal expansion (CTE) of the highest dense samples was measured by a dilatometer (NETZSCH, DIL 402) up to 800 °C with a heating rate of 10 °C min^{-1}.

2.2. Electrical and electrochemical characterizations of SP synthesized cathode powder

Electrical conductivities of the sintered samples (sintered in the range of 900–1100 °C at an interval of 100 °C) were measured in the temperature range 500–800 °C in air at an interval of 25 °C, using standard 4-probe DC measurement technique using an 8½ digit multimeter (Keithley, 2002). AC complex impedance spectroscopy was used to measure the effective interfacial polarization along with oxygen reduction kinetics of such cathodes materials in the form of screen printed layers onto gadolinium doped ceria (CGO)-based electrolyte using symmetrical cell configuration (LSCF/CGO/LSCF). The measurements were made by applying a small amplitude AC voltage (0.1 V) to the cell and monitoring the response current as a function of the AC frequency ($10^{-1} \leq f \leq 10^{6}$ Hz). Impedance measurements were carried out in the temperature range of 500–800 °C at a regular interval of 50 °C for all the samples using a Solartron Analytical Frequency Response Analyzer (Solartron 1260 A, UK).

2.3. Single cell fabrication and electrochemical testing

Anode-supported half cells with thin film of 8 mol % of yttria stabilized zirconia (YSZ) electrolyte layer (~20 μm) having configuration of nickel oxide (NiO)–YSZ/YSZ were screen printed with the optimized LSCF cathode. The optimization of the LSCF cathode was envisaged from the EIS spectroscopic measurement in conjugation with CGO based interlayer and thus the ultimate single cell configuration was found to be NiO–YSZ/YSZ/CGO/LSCF. The detailed description of cell fabrication process is described in our earlier work [5,37]. *I–V* characteristics of such single cells were carried out in the form of button cells of ~16 mm diameter with an active area of ~0.3 cm^2 in the temperature of 700–800 °C using

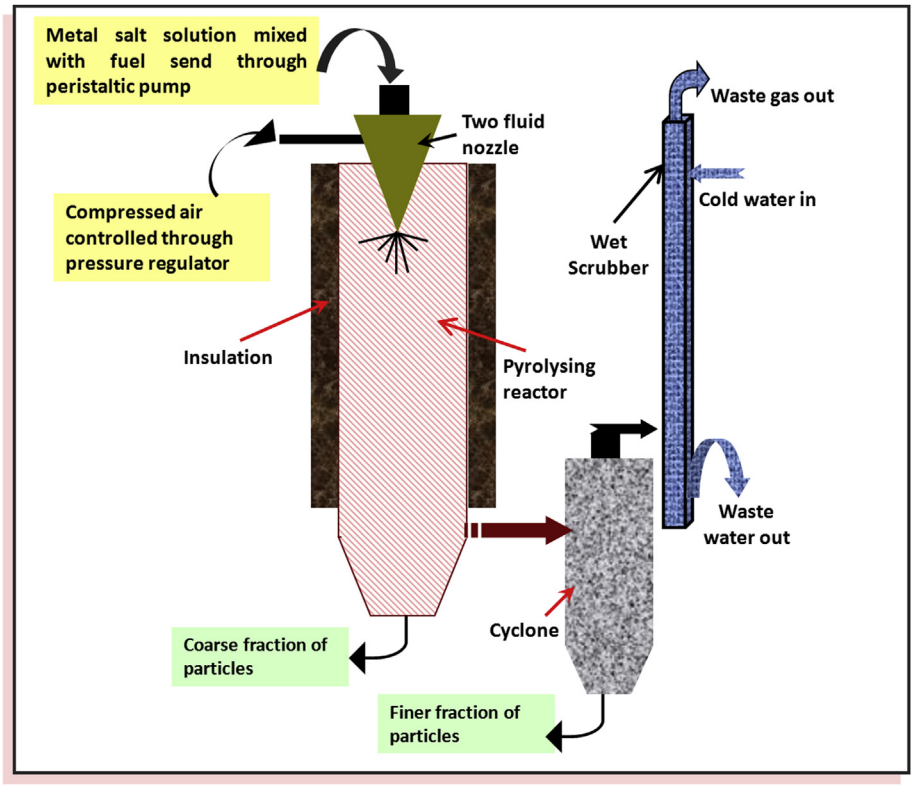

Fig. 1. Schematic of spray pyrolysis technique.

current collector as Pt-mesh (mesh size 250) connected with Pt-lead wire of ~0.3 mm on both the sides of the electrodes. The anode side is fed with moist hydrogen (3% of H_2O) and the cathode is fed with oxygen or air with individual flow rates of 100 SCCM (for hydrogen and oxygen) and 500 SCCM for air. Endurance test of the button cells with optimized LSCF-based cathode compositions were carried out for a span of 500 h under different electronic loads of 0.5 A cm^{-2} and 1.0 A cm^{-2} (Amrel ZVL, USA) using hydrogen as the fuel and oxygen as the oxidant.

3. Results and discussion

3.1. Thermal characterization of the precursor gels

Fig. 2a represents the thermogravimetric analysis of LSCF based complex gel of different compositions (without any solid loading) prepared using glycine as the single fuel. In case of all the samples, it has been observed that after an initial small weight loss in the temperature range of 65–140 °C, a major sharp single stage weight loss occurs below 165–225 °C based on the precursor gel composition. The initial small weight loss is due to the evaporation of trapped water. The sharp weight loss at ~200 °C results from the decomposition of respective glycine–metal nitrate complexes. The weight loss continues up to ~450 °C at a slow but steady rate and thereafter no significant weight loss is observed. The compositions, LSCF-5 and LSCF-6 shows sharper decomposition at the beginning followed by a relatively sluggish rate using glycine as the fuel which seems to be ideal for the decomposition of metal nitrate precursor salt solution by SP technique. It is worth to control the exothermicity of the reaction or decomposition, since solvent core evaporation is followed by the solute drag and subsequent precipitation inside the solvated droplets during the flight of atomized droplet in spray pyrolysis technique [32,35]. This helps in the attainment of relatively higher residence time for the desired growth of the primary nanoparticulates formed in-situ during the pyrolyzing chamber. Fig. 2b shows the comparative thermal decomposition behaviors of complex gel of composition LSCF-5 and LSCF-6 using citric acid and glycine (mixture ratio is 1:1) as the mixed fuel. Combination of these fuels results in a second stage decomposition in the temperature range of 210 °C–450 °C and responsible for higher residence of the metal ion–chelate complex before final decomposition. Thus, it is expected to favor the particle growth after the solvent core evaporation of the atomized droplets during the pyrolysis process. It is evident from Fig. 2b that, addition of citric acid controls the exothermicity of the reaction. Therefore, combination of citric acid and glycine leads to optimum exothermicity during gel decomposition. Hence, all the cathode compositions as reported under this investigation are considered to be pyrolyzed with the combination of mixed fuel.

3.2. Powder characterization

Fig. 3 shows the X-ray diffraction (XRD) patterns of the SP LCSF based cathode compositions calcined at 800 °C. The phase analyses of the diffractograms reveal that, irrespective of the dopant concentration either in 'A' or in 'B' site, the perovskite structure (ABO_3) of LSCF-1 to LSCF-6 is completely rhombohedral in nature. The average crystallite sizes of spray pyrolyzed LSCF based cathode powders are found to be 30–50 nm. It can be observed form Fig. 3 that the XRD peaks of LSCF-1 shift slightly to higher angles. This could be explained on the fact that, for LSCF-1 with higher Co content, the lattice shrinkage results with subsequent substitution of smaller Co^{3+} for Fe^{3+} in the B-site [18,34]. This tends to shift the peak positions to higher angles in LSCF-1. Contrary to LSCF-1, other Co-rich compositions viz. LSCF-3 and LSCF-5 do not appear to follow such trend. The expansion effect of larger Sr^{2+} replacing La^{3+} is compensated by the shrinkage effect of an increase in the average valence of B-site cations [20,38]. Such counteractive effect tends to maintain a constant cell volume and thereby the diffractions are observed at identical angles for all compositions LSCF-2 to LSCF-6. The aforementioned phenomena could also be proved from the calculated lattice parameters. All LSCF compositions except LSCF-1 exhibit lattice parameters of $a = b = 5.352$ Å and $c = 13.244$ Å. Around 5% deviation is observed in the magnitude of 'a (i.e. equal to b)' for LSCF-1 without any significant variation in the value of 'c'. The lattice parameters of LSCF-1 are found to be $a = b = 5.102$ Å and $c = 13.244$ Å. It is interesting to observe that almost 90% phase purity is attained in the as-synthesized condition for all the LSCF-based materials synthesized with mixed fuel (Fig. 3). The controlled exothermicity during the pyrolysis process of the atomized droplets using such mixed fuel help in the formation of effective primary nanocrystallites and resulted in phase pure LSCF-based cathodes. Fig. 4a shows the FESEM micrograph of LSCF-based samples substituted with maximum Sr at the 'A' site with highest Co/Fe ratio (LSCF-5). The micrographs reveal the nanostructured fragmented shell particles with smaller granular shape of the as-sprayed powder. The batch prepared with 25 wt. % of solid loading of LSCF-5 ash favor the in-situ growth of the particulates as observed in Fig. 4b. The micrograph reveals the secondary mesoporous micro spheres are grown in-situ during the pyrolysis process consisting of primary nanoparticulates embedded within the granules. Spray pyrolysis is an auto-ignition induced process capable of controlling the exothermic redox reaction between the anions of metal salt and the mixed fuel (glycine and citric acid, in

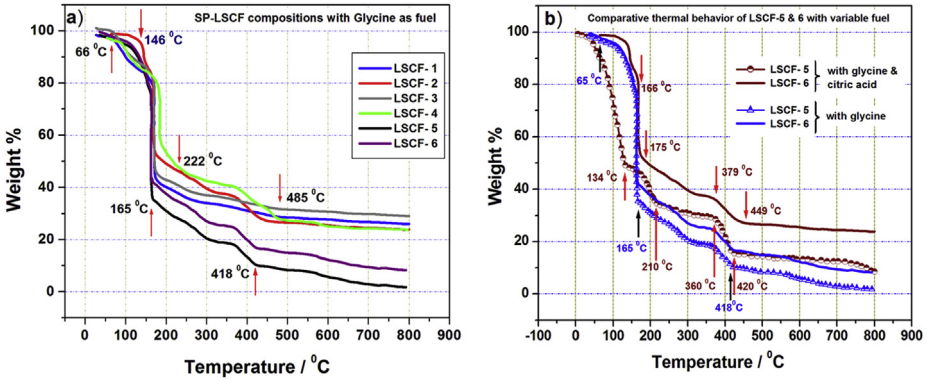

Fig. 2. Thermogravimetric analysis of: a) SP-LSCF compositions with glycine as fuel and b) LCSF-5 and LSCF-6 with combined fuels of glycine and citric acid.

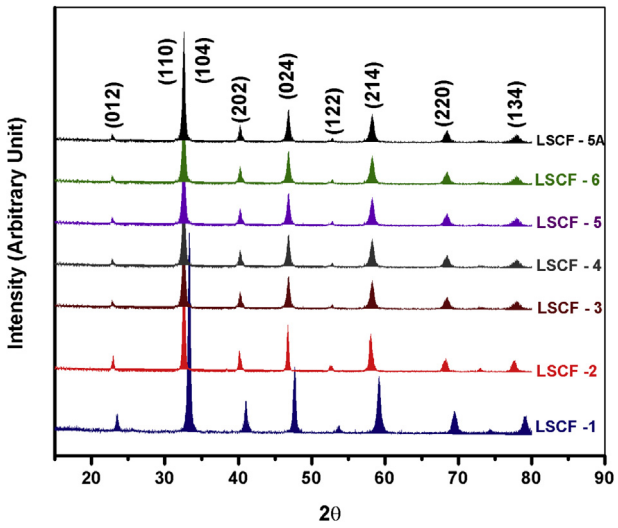

Fig. 3. X-Ray diffractograms of SP-LSCF powders of variable compositions calcined at 800 °C.

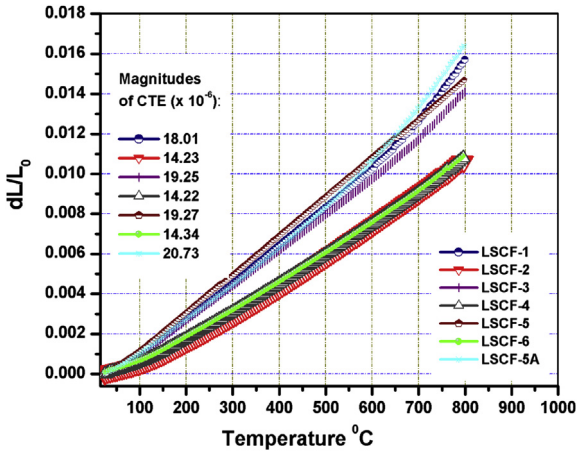

Fig. 5. Coefficient of thermal expansion (CTE) of SP-LSCF compositions.

particular). Such feature leads to a self-propagating auto ignition reaction within individual droplets for generating nanoparticulates having compositional homogeneity. Therefore, it is worth to note that the controlled exothermicity of mixed fuel and definite percentage of solid loading of precalcined ashes as the seeding agent helps in pertinent nanoparticle growth with in-built mesoporosity which might be quite effective for utilizing as the porous cathode layer for developing high performance SOFC.

3.3. Thermal and electrical characterizations of SP-synthesized sintered LSCF cathodes

The coefficient of thermal expansion (CTE) of LSCF based SP cathodes is studied with the dense bulk sample sintered at 1100 °C for 4 h having >98% densification. CTE is measured from room temperature to 800 °C in air and the behavior is shown in Fig. 5. Irrespective of composition, all the curves show a linear relation between temperature and thermal expansion. It is observed that, the CTE values are high with higher Co-doping at the 'B' site of lanthanum ferrites compared to the higher Fe-content at the same site of the perovskite. The values of the CTEs as derived from the slope of the graph are also given in Fig. 5. The magnitudes of CTEs are ranging from 14×10^{-6} K^{-1} to 20×10^{-6} K^{-1} based on the doping concentrations of the 'A' and 'B' sites of the perovskites. The magnitudes of CTE as obtained for variable LSCF compositions in the present investigation are also supported by the findings of prior literature [39,40]. As envisaged from Fig. 5, Co-rich lanthanum ferrite cathodes often exhibit higher CTEs and cause hairline cracks at the cathode/electrolyte interface. Such a higher mismatch of CTEs of these cathodes with YSZ electrolyte may, however, be minimized by suitable use of doped ceria based interlayer [41].

Fig. 6 shows the temperature dependence of electrical conductivity measured between 500 °C and 800 °C. Although, the synthesized SP-LSCF samples are sintered in the range of 900–1100 °C, but in the present context temperature dependent conductivities are reported for those LSCF-compositions which are sintered at 1100 °C. Among the Co rich LSCF-compositions, except LSCF-1, other samples (LSCF-3 and LSCF-5) show metallic type of conductivity. The compositions, LSCF-3 ($La_{0.65}Sr_{0.3}Co_{0.8}Fe_{0.2}O_{3-\delta}$) and LSCF-4 ($La_{0.65}Sr_{0.3}Co_{0.2}Fe_{0.8}O_{3-\delta}$), with an off-stoichiometric Sr-content are expected to enhance the oxide ion conductivity due to the presence of additional oxygen vacancies within the lattice. The conductivities of LSCF-2 and LSCF-4 are purely semiconducting, whereas, LSCF-6 shows a transforming nature of semiconducting to metallic behavior upon increasing the temperature. It has been reported that such type of transformation normally occurs at ≥40 mol percentage of Sr substitution in the La-site [42]. The composition LSCF-6 sintered at 1100 °C, exhibit a thermally activated semiconducting behavior at lower temperatures (<600 °C). Electrical conductivity, however, decreases with increase in temperature above the transition temperature. The formation of oxide ion vacancies accompanied by a reduction of Fe^{3+} to Fe^{2+} or Co^{3+} to

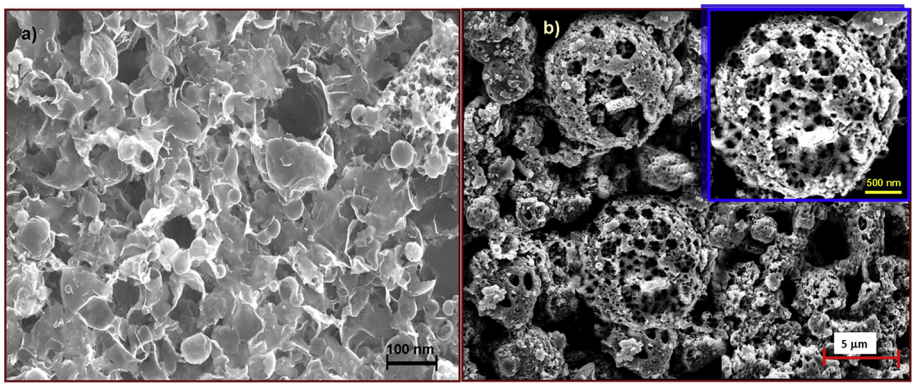

Fig. 4. FESEM micrographs of calcined powders: a) LSCF-5 (as synthesized) and b) LSCF-5A (in-situ growth after solid loading).

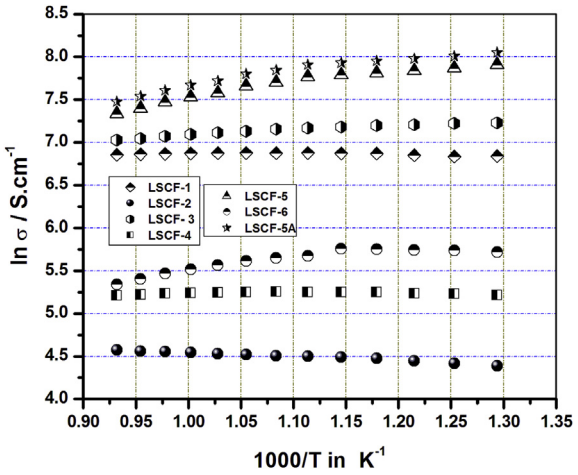

Fig. 6. Temperature dependent electrical conductivities of SP-LSCF compositions sintered at 1100 °C.

Co^{2+} at higher temperatures are the main causes for generation and loss of charge carrier concentration resulting in a slight decrease in conductivity [43]. Lee and Manthiram [44] reported that the transition temperature (300–500 °C) from semiconducting to metallic behavior decreases with increasing cobalt content. From the 'B' site dopant of the perovskite, a relatively higher Co/Fe ratio provides superior conductivity. A charge disproportionation of Co^{3+} ($2Co^{3+} \rightarrow Co^{4+} + Co^{2+}$) occurs in $La_{1-x}Sr_xCo_{1-y}Fe_yO_{3-\delta}$, based compositions, which increases the concentration of electronic carriers [42]. The denser microstructure of the Co-rich compositions benefits the conduction of electrical carriers. The highest value for the electrical conductivity is achieved with composition LSCF-5 sintered at 1100 °C and the value is found to be ~1500 S cm^{-1}. Not much variation with respect to the electrical conductivity is observed for LSCF-5A composition upon subsequent growth of particulates inside the reactor by adding suitable seeding agent in the form of precalcined ashes. The activation energies either in the semiconducting or metallic region are calculated from the Arrhenius plots of electrical conductivity of SP-LSCF compositions from the corresponding slopes of the graphs using their respective linear fits and are given in Table 2. Almost temperature independent behavior for electrical conductivity for LSCF-4 is established by the least activation energy for electrical conduction (~0.05 kJ mol^{-1}). The highest activation energy is found for LSCF-5A (~12.8 kJ mol^{-1}) having highest electrical conduction. It is found that spray pyrolyzed LSCF cathode materials having metallic conduction exhibit higher activation energy barrier for electrical conduction compared to that of semiconductor behaviors. Activation barrier though correlated with electrical conduction, the required magnitude is however dependent on processing techniques, compositions etc. The rate of change in conduction with temperature is negligible for LSCF-4. In contrast, LSCF-5A with higher Co content and exhibiting metallic conduction, is found with highest conductivity with sharp change in conduction with variation in temperature.

Table 2
The activation energies of the SP-LSCF based compositions.

Sl. No	Sample ID	Activation energy (kJ mol^{-1}) [Sintering temperature = 1100 °C]	
1	LSCF-1	0.52	
2	LSCF-2	3.96	
3	LSCF-3	4.68	
4	LSCF-4	0.05	
5	LSCF-5	12.89	
6	LSCF-6	Semi-conducting region 1.97	Metallic region 15.39
7	LSCF-5A	12.87	

3.4. Impedance spectroscopy of SP-synthesized cathodes in the form of thick films

The interfacial polarizations of LSCF-based cathode have been carried out onto CGO-based electrolyte in the form of LSCF/CGO/LSCF symmetrical cell configuration. The cathodes are screen printed with an average thickness of ~50 μm and sintered in the temperature range of 900–1100 °C with an interval of 100 °C. Fig. 7 shows characteristics impedance spectra of highest conducting cathode (LSCF-5) which reveal the temperature dependence of cathode polarization resistance measured at 800 °C as a function of cathode sintering temperature. The calculated values of polarization resistance for all the composition derived from their respective impedance spectra measured at 800 °C are given in Table 3. It is observed that with increase in cathode sintering temperature from 900 °C to 1000 °C, difference in cathode polarization (R_p) is not significant enough when measured in static air. The polarization resistance (R_p) is found to be the highest for Co lean composition of LSCF-2 (0.447 Ω cm^2) and the lowest for Co rich composition of LSCF-5 (0.091 Ω cm^2), both being sintered at 900 °C and measured at 800 °C. The trend for magnitudes of R_p is in the order: $R_{pLSCF\text{-}5} < R_{pLSCF\text{-}6} < R_{pLSCF\text{-}3} < R_{pLSCF\text{-}4} < R_{pLSCF\text{-}1} < R_{pLSCF\text{-}2}$. It is found that higher Co/Fe ratio results in lower cathode interfacial polarization, however, the dopant concentration at the 'A' site has a higher impact on the final value if the percentage doping is found to be ≥40 mol % of Sr in La site. Minor increase in cathode overpotential is found with increase in sintering temperature from 900 °C to 1000 °C. In the present study, the magnitude of overpotential for LSCF-5 increases from 0.091 Ω cm^2 to 0.18 Ω cm^2 with the increase in sintering temperature from 900 °C to 1000 °C. A steep increase in cathode interfacial polarization over the sintering temperature of 1000 °C is observed for LSCF-5 and the highest value of 0.72 Ω cm^2 is obtained for cathode sintering temperature of 1100 °C. This could be due to the collapse of the near net structure of SP-LSCF compositions during high temperature sintering. As envisaged from Fig. 4b, the mesoporous cathode (LSCF-5A) synthesized by inducing seeding agent in the form of precalcined ashes to the batch of LSCF-5, causes the overall cathode interfacial polarization to drop down to 0.032 Ω cm^2 at 800 °C for the cathode sintered at 900 °C. The interfacial polarization is found to remain almost constant (0.032 Ω cm^2–0.057 Ω cm^2) in the range of cathode sintering temperature of 900–1000 °C. This is primarily attributed to the interconnected mesoporosity of the particulates synthesized under the novel condition of spray pyrolysis technique, owing to which the diffusion polarization reduces at higher cathode sintering temperature. Drastic increment of R_p for LSCF-5A (0.43 Ω cm^2) is, however, observed at cathode sintering temperature of 1100 °C which could be because of structural disability by coagulation of the meso pores at such higher cathode sintering temperature. Fig. 8a–c illustrates the microstructure of CGO based symmetric cells synthesized with SP-LSCF cathode (LSCF-5) sintered at 900 °C, 1000 °C and 1100 °C respectively. It is clearly observed that near net shape cathode microstructure is more prevalent with the cathode sintered at 900 °C and retains till 1000 °C. The cathode structure collapses completely at 1100 °C leaving behind almost no interlinking porosity within the sintered grains of the pyrolyzed cathode. Thus, the cathode diffusion polarization is believed to be lowest at 900 °C and maximum at 1100 °C which resembles the findings of cathodic overpotential as envisaged from the impedance spectra (Fig. 7). Fig. 8d shows the retention of interconnected

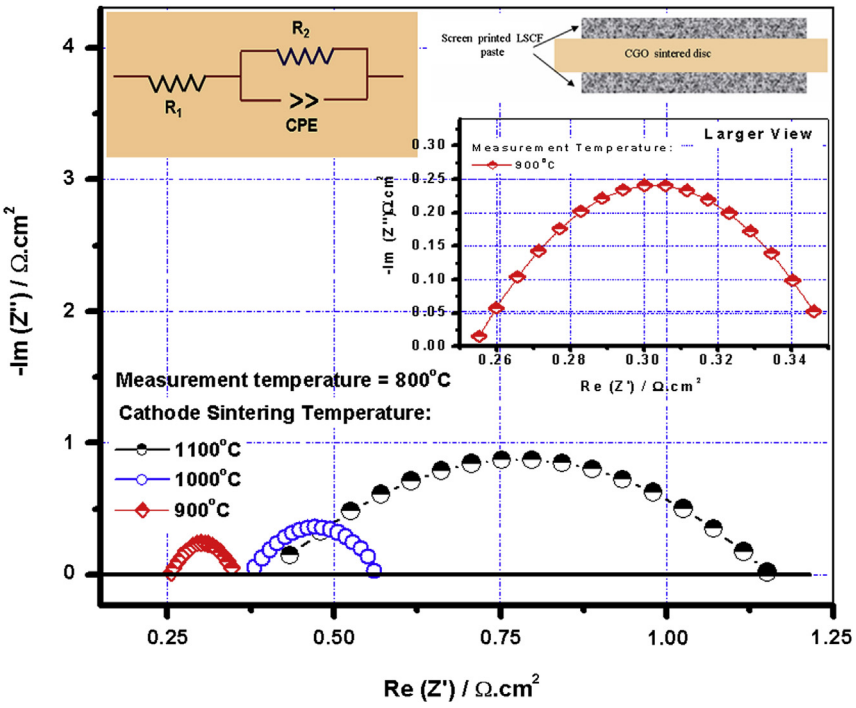

Fig. 7. Dependence of impedance spectra for LSCF-5 measured at 800 °C with variation of sintering temperature.

mesoporous microstructure of LSCF-5A till 1000 °C. LSCF-5A being synthesized by in-situ growth of precalcined ashes added as the seeding agents corroborates well with the unaltered cathode polarizations as observed for such cathode in the sintering temperature range of 900–1000 °C.

Fig. 9a exhibits the variation of cathode polarizations (R_p) with the measurement temperature ranging from 500 to 800 °C for the SP-cathodes sintered at 900 °C. It is observed that in the temperature range of 700–800 °C, variation of cathode polarization with temperature is insignificant for all SP-LSCF cathode compositions. The lowest value is still, however, observed for LSCF-5 composition in the entire temperature range of 500–800 °C and the magnitude is found to be 57.49 Ω cm^2 and 0.091 Ω cm^2 at 500 °C and 800 °C respectively. Cathode polarizations of SP-LSCF having compositions of LSCF-1, LSCF-2 and LSCF-4 show a stepper rise in the cathodic resistances at and below 550 °C. LSCF-5A prepared by in-situ seeding of the precalcined ashes during the pyrolysis is found to exhibit almost linear relationship with minimum variation in cathode polarization in the temperature range of 500–800 °C. The magnitude of the cathode polarization for LSCF-5A in this temperature range is found to vary from 0.16 Ω cm^2 to 0.032 Ω cm^2. Fleig [45] summarized two possible paths for cathodic reaction viz. electrode surface path for electronic conductor (e.g. LSM) and bulk path for MIEC-based cathode (e.g. LSCF). Williford et al. [46] further established that cathode reaction through the bulk path could be accelerated by tailoring the morphology of MIEC cathode in terms of optimized porosity. It has been mathematically established that, the molecular flux through pores (I_g) is inversely proportional to the tortuosity for diffusion of gas in pores (τ_g) and ionic current (I_p) is also inversely proportional to the solid tortuosity (τ_s) for electronic and ionic conduction. In addition, tortuosity for diffusion of gas in pores (τ_g) varies inversely with the porosity [46]. Hence, optimization of porosity within MIEC cathode microstructure is the prime requisite which controls the overall molecular flux for augmentation of ionic current from electrode to electrolyte surface. In the present investigation, the morphologically architectured LSCF-5A possesses in-build mesoporosity that has been developed by external seeding during spray pyrolysis technique. This helps not only in intimate contacts of the LSCF grains but also builds proper porosity within the granules leading to effective electrochemical reduction of the oxidants at the TPB regions. Such morphological architecture in LSCF-5A compared to LSCF-5 is found to remain intact even in the screen printed thick layers when applied onto the CGO-based symmetric cells. This typical microstructure of the cathode results in extension of TPB preferably through the bulk path and thereby reduces the polarization losses for oxide ion transport from electrode surface to the electrolyte. Fig. 9b depicts the Arrhenius plot of cathode polarizations as a function of temperature for SP-LSCF cathodes. All the cathode compositions exhibit a linear relation in the Arrhenius plots. The activation energies as calculated from the slope of Fig. 9b for all the cathode compositions ranges in between 61 and 68 kJ mol^{-1} with minimum value observed for LSCF-5A (15.39 kJ mol^{-1}). The aforementioned findings emphasizes that tailoring of the particulate morphology by in-situ growth of the nanoparticulates during SP helps in reducing the

Table 3
Dependence of polarization resistance (R_p) measured at 800 °C from impedance spectra of SP-LSCF based compositions on cathode sintering temperature.

Sl. No	Sample ID	Cathode sintering temperature (°C)		
		900	1000	1100
		Polarization resistance (R_p) [Ω cm^2]		
1	LSCF-1	0.316	0.448	1.337
2	LSCF-2	0.447	0.592	1.478
3	LSCF-3	0.126	0.221	0.907
4	LSCF-4	0.181	0.247	0.978
5	LSCF-5	0.091	0.18	0.72
6	LSCF-6	0.108	0.203	0.815
7	LSCF-5A	0.032	0.057	0.43

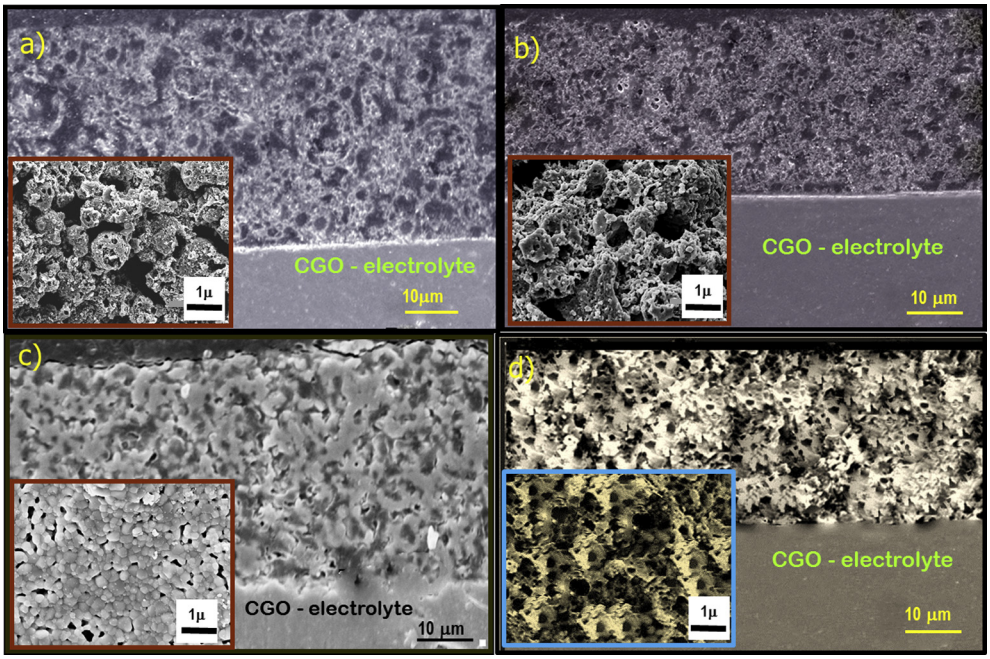

Fig. 8. SEM of CGO-based symmetric half cells synthesized with: LSCF-5 (a–c); sintered at a) 900 °C, b) 1000 °C, c) 1100 °C and d) LSCF-5A sintered at 1000 °C (*insets represent the cathode microstructure at a larger magnification*).

cathode polarization with lowest activation energy. In addition, such superior functionalities ensure better compatibility of LSCF for the application of cathode in the temperature range of 500–800 °C.

3.5. Electrochemical activity for oxygen reduction reaction (ORR) for spray pyrolyzed LSCF cathodes derived from impedance spectroscopy

The exchange current density (i_0) for such spray pyrolyzed LSCF cathode sintered at 900 °C is obtained from AC impedance spectroscopy. The equivalent circuit of Fig. 7 (inset) clearly demonstrates that, the overall impedance spectra for the present system can be analyzed using resistive contributions from the contacts, leads, resistance part of the working electrode (WE), reference electrode (RE), designated as R1 and from ORR polarization resistances (R2) with constant phase elements (CPE). Based on the proposition of Liu et al. [47], exchange current density (i_0) can be obtained from the following equation: $I_0 = RT\,\nu/nFR_p$, where R, T, ν, n, R_p and F are the gas constant, absolute temperature, number of occurrences of the rate limiting steps, number of electrons transferred for the ORR, cathode polarization resistance and Faraday constant respectively. In case of LSCF based cathode, 'n' and 'ν' happens to be 4 and 1 respectively because the total number of electrons transferred per oxygen molecule being 4 and rate limiting steps would be unique [48]. The magnitudes of exchange current densities in the temperature regime of 500–800 °C for all the SP-LSCF compositions are calculated from the above equation and are shown in Fig. 10a and b. LSCF-5 is found to exhibit maximum exchange current density of ~253.4 mA cm^{-2} at 800 °C and ~23.4 mA cm^{-2} at 700 °C among all the SP-LSCF. It is further observed from Fig. 10b that LSCF-5A which is synthesized with tailored particulate morphology by in-situ seeding during the pyrolysis process has the best effectivity towards the ORR of such cathode having the highest exchange current density of ~722 mA cm^{-2} at 800 °C. As envisaged from Fig. 9a, variation of the interfacial polarization for such cathode is very marginal in the

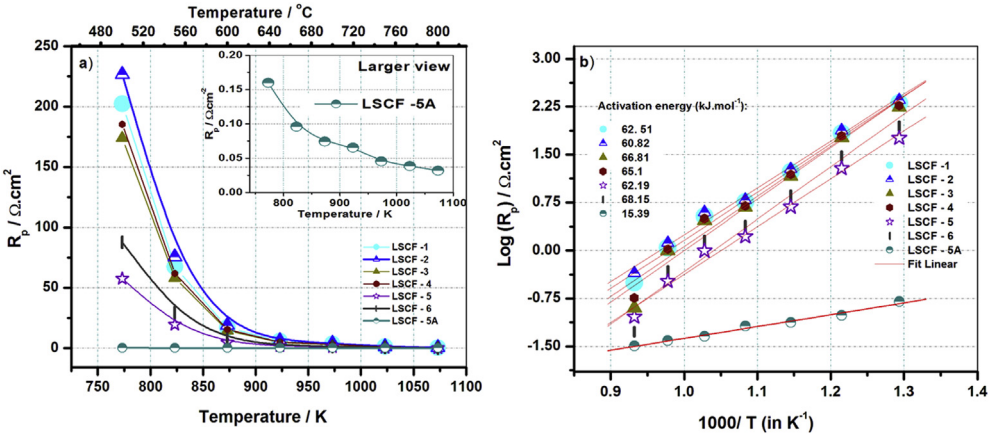

Fig. 9. Variation of cathode polarizations (R_p) in measurement temperature range of 500–800 °C (a) and Arrhenius plot of cathode polarizations as a function of temperature (b) for SP-LSCF cathodes.

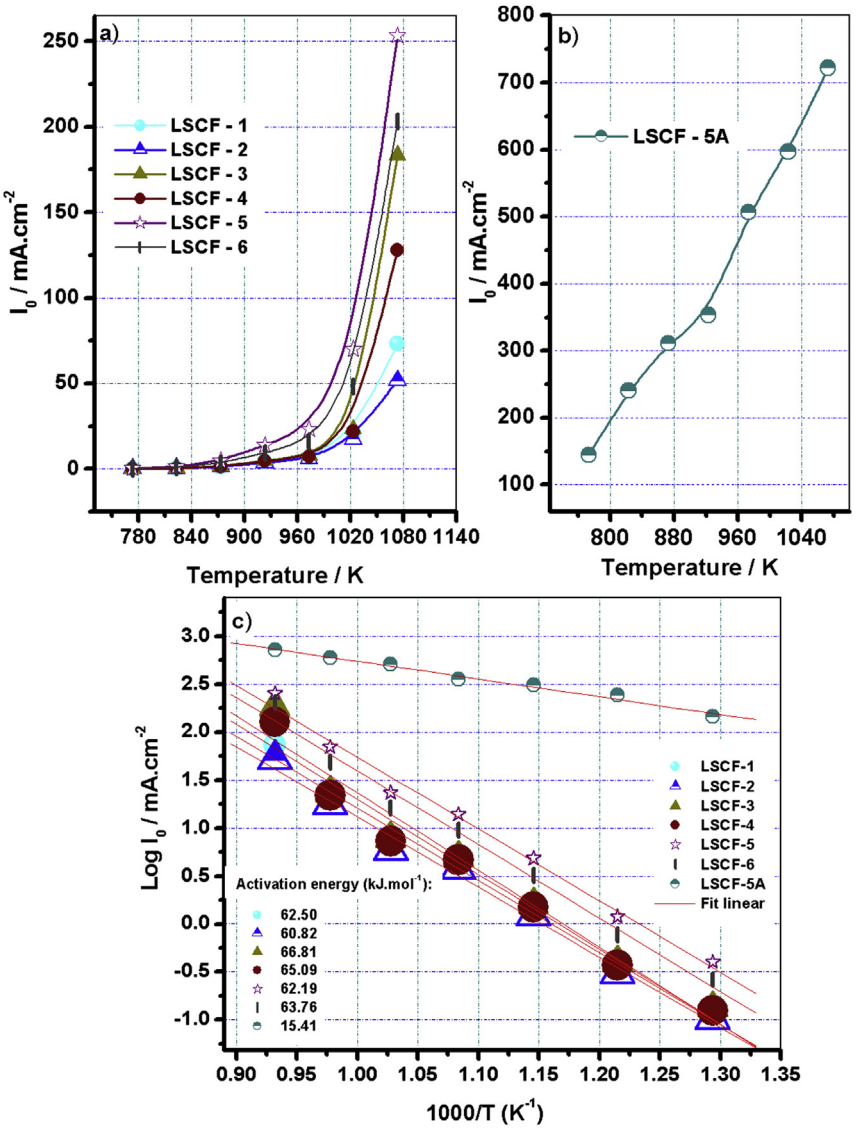

Fig. 10. Dependence of exchange current density (I_0) on temperature variation (a, b) and Arrhenius plot of exchange current density as a function of temperature for all LSCF-compositions (c).

temperature regime of 500–800 °C. Exchange current density for LSCF-5A is found to vary a little in the aforementioned temperature range with a magnitude of ~507 mA cm^{-2} at 700 °C. Owing to such facts, LSCF-5A with interconnected mesoporosity and micron sized spherical granules having primary nanoparticulates embedded within could be a better option for application in the range of 700–750 °C for IT-SOFC. Fig. 10c shows the Arrhenius plot of exchange current density as a function of temperature which is found to be linear for all the experimental SP-LSCF compositions. It is observed that all the LSCF compositions exhibit activation energy for cathodic ORR in the range of 60–67 kJ mol^{-1}. Significant low activation energy of 15.41 kJ mol^{-1} for cathode ORR is observed for LSCF-5A which resembles with the cathodic ORR values for such compositions in the temperature range of 500–800 °C.

3.6. Electrochemical performance and endurance test of solid oxide fuel cell with optimized cathodes

The polarization behavior of variable cathode compositions used for symmetric cell testing (Sections 3.3 and 3.4) describes the importance of compositional divergence and morphology for the application of SP-LSCF-based MIEC cathode in conjunction with gadolinium doped (CGO) ceria based interlayer in SOFC. Fig. 11a–d shows the comparative plots for the current density versus cell voltage (I–V) behavior of anode-supported button cells fabricated using selected cathode compositions viz. LSCF-5 (CELL-A) and LSCF-5A (CELL-B) having cell structure of NiO–YSZ/YSZ/CGO/LSCF-5/5A. CELL-A and CELL-B are measured for their electrochemical activities in the temperature range of 700–800 °C with an interval of 50 °C. Significant enhancement in the cell performance is observed for CELL-A compared to that of the button cells fabricated with LSCF synthesized by combustion technique as reported in our earlier communication [33]. An approximate 50% augmentation of current density (3.5 A cm^{-2} at 800 °C and 0.7 V) is achieved for CELL-A compared to the current density (1.7 A cm^{-2} at 800 °C and 0.7 V) obtained for button cells prepared with LSCF cathode synthesized by liquid combustion technique. This may be attributed to the fact that LSCF-5 composition synthesized by SP-technique is composed of homogenously distributed nanocrystalline doped lanthanum ferrite particles with interconnected porosity compared to that synthesized by solution combustion. CELL-A exhibits current density of 2.1 A cm^{-2} and 1.2 A cm^{-2} at a temperature of 750 °C and

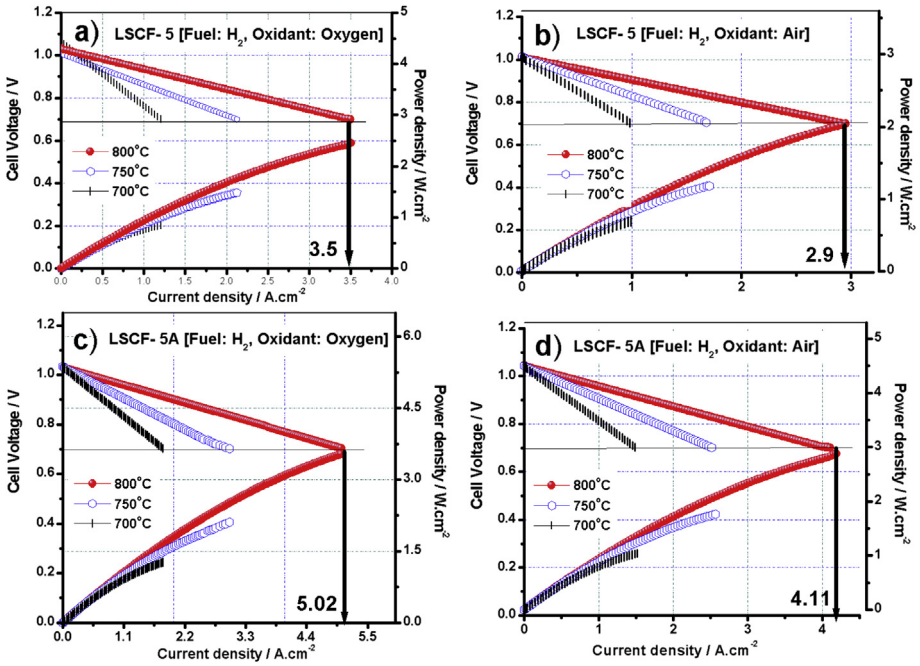

Fig. 11. Electrochemical performances of button cells: a) and c) with oxygen and hydrogen having LSCF-5 and LSCF-5A cathodes respectively; b) and d) with air and hydrogen having LSCF-5 and LSCF-5A cathodes respectively.

700 °C respectively at 0.7 V with oxygen as oxidant. The performance of CELL-A with air as the oxidant shows a drop of ~18% with respect to the peak current derived out of the cell and the current densities of such cell are found to be ~2.9 A cm^{-2}, ~1.68 A cm^{-2} and ~0.98 7 A cm^{-2} at 800 °C, 750 °C and 700 °C respectively at 0.7 V (Fig. 11b). The cell configuration with LSCF-5A (CELL-B) shows a dramatic increase in the current density to ~5.0 A cm^{-2} and ~4.1 A cm^{-2} at 800 °C at 0.7 V (with hydrogen as fuel and oxygen and air as oxidants respectively as shown in Fig. 11c and d). Morphologically tailored particulates with in-built mesoporosity and nanocrystalline nature in LSCF-5A cause such multifold increment in electrochemical performance. CELL-B exhibits current density of 3.0 A cm^{-2} and 1.8 A cm^{-2} with oxygen and 2.5 A cm^{-2} and 1.48 A cm^{-2} with air as oxidant at 750 °C and 700 °C respectively at 0.7 V. The cell area specific resistances (ASR) are calculated from the linear portion of the *I–V* curves and the same is found to be the lowest for cells with LSCF-5A (0.065 Ω cm^2 at 800 °C) with oxygen as the oxidant. The cell ASR for CELL-A and CELL-B using hydrogen as fuel and oxygen and air as the oxidants are tabulated in Table 4. Microstructural control of the LSCF cathodes during pyrolysis reduces the cell ASR dramatically and thereby increases the cell performances significantly.

The time dependant endurance test related to cathode degradation for LSCF-5 and LSCF-5A are given in Fig. 12. The endurance test was carried out at 800 °C using hydrogen as fuel and oxygen as the oxidant. It is observed from figure (Fig. 12a) that upto a total time span of 500 h, degradation for the area specific resistance (ASR) of the cells are found to be 82.54 mΩ cm^2 and 75.84 mΩ cm^2 1000 h^{-1} under the applied current density of 0.5 A cm^{-2} for the electrode of composition of LSCF-5 and LSCF-5A respectively. During the same time span of initial 500 h, the degradation of the cell ASR is found to be 93.22 mΩ cm^2 and 78.06 mΩ cm^2 1000 h^{-1} for the electrodes of composition LSCF-5 and LSCF-5A with the circuit load of 1.0 A cm^{-2}. The percentage degradation for such LSCF-based composition is calculated to be 4.2% and 3.8% 1000 h^{-1} for LSCF-5 and LSCF-5A with an electronic load of 0.5 A cm^{-2} and 10% and 8.9% 1000 h^{-1} for the same compositions under the load of 1.0 A cm^{-2} for the cells tested till 500 h. It is observed that the degradation rate of the cell using such cathode is found to be still lower as reported in literature with LSCF without any surface modification [49]. It is found in the literature that for a span of 500 h, current density degrades nearly ~16% over a span of 500 h. High doping level of ceria by La and Ca (i.e. 50% mol. total substitution) creates high surface oxygen vacancy concentration. It has also been observed that LSCF cathode when modified by a thin coating made of lanthanum calcium cobaltite (LCC), oxygen vacancy concentration may increase at the surface layer having higher rate of dissociation of oxygen molecule into atomic oxygen [49,50]. This phenomenon helps in facilitating the oxygen reduction reaction. The LCC coating onto the parent LSCF based cathode can also reduce Sr enrichment at the LSCF/CGO or SDC interface and makes partially responsible for preventing the cathode degradation [51]. It has also been reported that either Gd or Sm doped ceria shows excellent solubility towards the SrO [52] and thereby reduces the

Table 4
Dependence of cell area specific resistance at variable operating temperatures on cathode composition and characteristics (in all the cases H_2 is used as the fuel).

Sl. No	SOFC ID	Oxidant type	Operating temperature (°C)	Cell ASR (mΩ cm^{-2})
1	CELL-A	Oxygen	800	94.9
			750	145
			700	304
		Air	800	105
			750	180
			700	309
2	CELL-B	Oxygen	800	65.1
			750	112
			700	182
		Air	800	84.5
			750	134
			700	227

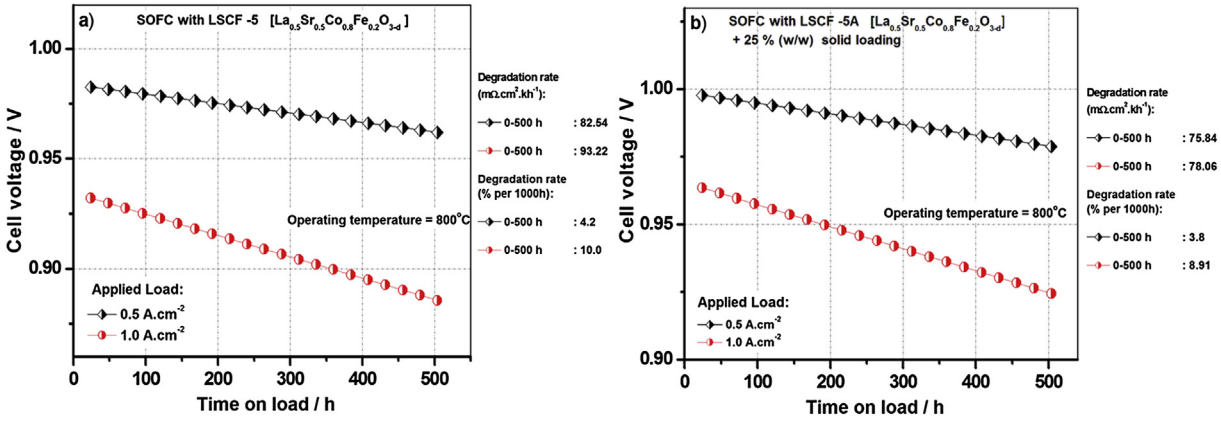

Fig. 12. Endurance test of button cells with: a) LSCF-5 and b) LSCF-5A measured for 500 h with different electronic loads of 0.5 A cm^{-2} and 1.0 A cm^{-2} using hydrogen and oxygen.

driving force of diffusion of Sr from the LSCF cathode to the YSZ electrolyte. This in turn helps in preventing the enrichment of Sr on LSCF grain surface keeping the active sites alive for oxygen reduction.

4. Conclusions

A novel spray pyrolysis (SP) technique is utilized for synthesizing nanocrystalline (~50 nm) doped lanthanum ferrite (LSCF) based mixed ionic and electronic conductor (MIEC) of variable compositions and particulate morphology for application as SOFC cathodes. Irrespective of the cathode compositions of the present investigation, $La_{1-x}Sr_xCo_{1-y}Fe_yO_{3-\delta}$ (where, $0 < x \leq 0.5$, $y = 0.2$ and 0.8), stable rhombohedral perovskite phase is identified for all the materials with almost 90% phase purity in the as-synthesized condition. Thermal characterization of the gels reveal that the addition of mixed fuel i.e. glycine and citric acid in 1:1 proportion results in effective decomposition which may lead to particle growth during pyrolysis. Thus, during pyrolysis, an attempt is pursued to add precalcined nanopowders of 0.25 M solution as the seeding agents to the precursor solution of same concentration. This seeding during pyrolysis process helps in in-situ homogeneous-homomolecular growth of the porous nanoparticulates inside the reactor. Significant growth of the nanoparticulates is observed with addition 25 wt. % of external nuclides in the form of precalcined ashes. Highest electrical conductivity of ~1500 S cm^{-1} is observed for $La_{0.5}Sr_{0.5}Co_{0.8}Fe_{0.2}O_3$ (LSCF-5) with higher Co/Fe ratio and with Sr doping of ≥40 mol% at 'A' site dopant. The higher ratio of Co/Fe leads to higher CTE (~20 × 10^{-6} K^{-1}) but the incompatibility is significantly compromised by the presence of gadolinium doped ceria (CGO) based interlayers. Cathode polarization (R_p) as envisaged from the impedance spectroscopy of CGO-based symmetric cell is found to be lowest (~0.09 Ω cm^2) for Co rich composition of LSCF-5 sintered at 900 °C. Conversely, highest cathode interfacial polarization (0.447 Ω cm^2) is observed for the Co lean composition of $La_{0.8}Sr_{0.2}Co_{0.2}Fe_{0.8}O_3$ (LSCF-2). A strong correlation of such low cathode polarization is found to be highly dependent on the cathode sintering temperature as well. A sharp enhancement in cathode interfacial polarization to 0.72 Ω cm^2 is observed for LSCF-5 cathode sintered at 1100 °C. Such increase could be attributed to the collapse of near net structure of SP-LSCF cathode materials upon high temperature sintering and is established from symmetric cell microstructure. SP cathode composition of $La_{0.5}Sr_{0.5}Co_{0.8}Fe_{0.2}O_3$ (LSCF-5A) that is synthesized by seeding agent for in-situ growth of the nanoparticulates, exhibits negligible dependence of cathode polarization on sintering temperature till 1050 °C. In addition, LSCF-5A also exhibits lowest activation energy for cathode polarization (15.39 kJ mol^{-1}). The exchange current densities as calculated from EIS, are found to be ~250 mA cm^{-2} at 800 °C and ~23. 4 mA cm^{-2} at 700 °C for LSCF-5 and maximizes to ~722 mA cm^{-2} at 800 °C with lowest activation energy of 15.41 kJ mol^{-1} for LSCF-5A. While significant augmentation of current density (3.5 A cm^{-2} at 800 °C and 0.7 V) is achieved for SP synthesized LSCF-5, the best performance is achieved from LSCF-5A with a current density as high as ~5.0 A cm^{-2} and ~4.0 A cm^{-2} at 800 °C at 0.7 V with hydrogen as fuel and oxygen or air as oxidants respectively. Endurance test of button cells till 500 h with SP synthesized LSCF-5A using hydrogen and oxygen reveals lowest degradation of 3.8% and 8.9% 1000 h^{-1} with the electronic loads of 0.5 A cm^{-2} and 1.0 A cm^{-2} respectively. SP synthesized LSCF-5A having tailored particulates with interconnected mesoporosity and embedded primary nanoparticles result in lower cathodic polarization and significant augmentation of the performance in the form of button cell.

Acknowledgments

The authors are grateful to the Director of the Institute for giving permission to publish this work. Technical assistance of Analytical Facility Division of the Institute for XRD and FESEM is acknowledged. Financial support from Council of Scientific and Industrial Research (CSIR), under NMITLI Project is also gratefully acknowledged.

References

[1] N.Q. Minh, J. Am. Ceram. Soc. 76 (1993) 563–588.
[2] S.P.S. Badwal, K. Foger, Ceram. Int. 22 (1996) 257–265.
[3] S.C. Singhal, K. Kendall, High Temperature Solid Oxide Fuel Cells; Fundamentals, Designs and Applications, Elsevier, 2003.
[4] R.N. Basu, Materials for Solid Oxide Fuel Cells in Recent Trends in Fuel Cell Science and Technology, Jointly Published by Anamaya Publisher and Springer, New Delhi (India) and New York, 2006, pp. 284–329.
[5] R.N. Basu, A. Das Sharma, A. Dutta, J. Mukhopadhyay, Int. J. Hydrogen Energy 33 (2008) 5748–5754.
[6] M. Liu, J. Winnick, Solid State Ionics 118 (1999) 11–21.
[7] J. Fleig, J. Power Sources 105 (2002) 228–238.
[8] D. Marinha, L. Dessemond, E. Djurado, J. Power Sources 197 (2012) 80–87.
[9] F. Qiang, K.N. Suna, N. Zhang, X.D. Zhua, S. Lea, D. Zhoua, J. Power Sources 168 (2007) 338–345.
[10] B.C.H. Steele, Solid State Ionics 94 (1997) 239–248.
[11] B. Wei, Z. Lu, X. Huang, J. Miao, X. Sha, X. Xin, W. Su, J. Eur. Ceram. Soc. 26 (2006) 2827–2832.
[12] S.B. Adler, Solid State Ionics 135 (2000) 603–612.
[13] M. Letilly, O. Joubert, L.G.L. Salle Annie, J. Power Sources 212 (2012) 161–168.
[14] S. Lee, Y. Lima, E.A. Lee, H.J. Hwang, J. Moon, J. Power Sources 157 (2006) 848–854.

[15] Z. Shao, S.M. Halle, Nature 431 (2004) 170–173.
[16] C. E-Schuck, A. Leonide, A. Weber, S. Uhlenbruck, F. Tietz, E. I-Tiffée, J. Power Sources 196 (2011) 7257–7262.
[17] T. Mitsui, A. Mineshige, T. Funahashi, H. Mieda, Y. Daiko, M. Kobune, H. Yoshioka, T. Yazawa, J. Power Sources 217 (2012) 170–174.
[18] E.D. Wachsman, K.T. Lee, Science 334 (2011) 935–939.
[19] F. Han, R. Mücke, T.V. Gestel, A. Leonide, N.H. Menzler, H.P. Buchkremer, D. Stöver, J. Power Sources 218 (2012) 157–162.
[20] L.W. Tai, M.M. Nasrallah, H.U. Anderson, D.M. Sparlin, S.R. Sehlin, Solid State Ionics 76 (1995) 273–283.
[21] J.A. Lane, S.J. Benson, D. Waller, J.A. Kilner, Solid State Ionics 121 (1999) 201–208.
[22] W.G. Wang, M. Mogensen, Solid State Ionics 176 (2005) 457–462.
[23] D. Mori, H. Oka, Y. Suzuki, N. Sonoyama, A. Yamada, R. Kanno, Y. Sumiya, N. Imanishi, Y. Takeda, Solid State Ionics 177 (2006) 535–540.
[24] M. Sase, J. Suzuki, K. Yashiro, T. Otake, A.I. Kaimai, T. Kawada, J. Mizusaki, H. Yugami, Solid State Ionics 177 (2006) 1961–1964.
[25] F. Deganello, V. Esposito, M. Miyayama, J. Electrochem. Soc. 154 (2007) A89–A96.
[26] S. Lee, H.S. Song, S.H. Hyun, J. Kim, J. Moon, J. Power Sources 187 (2009) 74–79.
[27] A.C. Johnson, B.K. Lai, H. Xiong, S. Ramanathan, J. Power Sources 186 (2009) 252–260.
[28] J. Hayd, L. Dieterle, U. Guntow, D. Gerthsen, E. Ivers-Tiffée, J. Power Sources 196 (2011) 7263–7270.
[29] J. Hayd, H. Yokokawa, E. Ivers-Tiffée, J. Electrochem. Soc. 160 (2013) F351–F359.
[30] C.Y. Fu, C.L. Chang, C.S. Hsu, B.H. Hwang, Mater. Chem. Phys. 91 (2005) 28–35.
[31] D. Beckel, A. Dubach, A.R. Studart, L.J. Gauckler, J. Electroceram. 16 (2006) 221–228.
[32] G.L. Messing, S.C. Zhang, G.V. Jayanthi, J. Am. Ceram. Soc. 76 (1993) 2707–2726.
[33] C.H. Chen, F.L. Yuan, J. Schoonman, Eur. J. Solid State Inorg. Chem. 35 (1998) 189–196.
[34] K. Okuyama, I.W. Lenggoro, Chem. Eng. Sci. 58 (2003) 537–547.
[35] S. Suda, M. Itagaki, E. Node, S. Takahashi, M. Kawano, H. Yoshida, T. Inagaki, J. Eur. Ceram. Soc. 26 (2006) 593–597.
[36] P. Pal, M.W. Raja, J. Mukhopadhyay, A. Dutta, S. Mahanty, R.N. Basu, H.S. Maiti, ECS Trans. 7 (2007) 1129–1138.
[37] A. Dutta, J. Mukhopadhyay, R.N. Basu, J. Eur. Ceram. Soc. 29 (2009) 2003–2011.
[38] L.W. Tai, M.M. Nasrallah, H.U. Anderson, D.M. Sparlin, S.R. Sehlin, Solid State Ionics 76 (1995) 259–271.
[39] A.O. Guimarães, A.M. Mansanares, V.F. Guimarães, H.R. Paes, H. Vargas, Appl. Phys. Lett. 102 (2013) 131910-1–131910-5.
[40] H. Ullman, N. Trofimenko, F. Tietz, D. Stöver, A. A-Khanlou, Solid State Ionics 138 (2000) 79–90.
[41] J.P. Martinez, D.M. Lopez, C.S. Baustista, A.J.D.S. Garcia, J.C.R. Morales, J.C. Vazque, P. Nunez, Bol. Soc. Esp. Ceram. 49 (2010) 15–22.
[42] H. Duanping, X.U. Qin, Z. Feng, C. Wen, L. Hanxing, Z. Jian, J. Wuhan Univ. Technol. Mater. Sci. Ed. 23 (2008) 80–84.
[43] Z. Yang, A.S. Harvey, A. Infortuna, J. Schoonman, L.J. Gauckler, J. Solid State Electrochem. 15 (2011) 277–284.
[44] K.T. Lee, A. Manthiram, Chem. Mater. 18 (2006) 1621–1626.
[45] J. Fleig, Annu. Rev. Mater. Res. 33 (2003) 361–382.
[46] R.E. Williford, P. Singh, J. Power Sources 128 (2004) 45–53.
[47] J. Liu, A.C. Co, S. Paulson, V.I. Birss, Solid State Ionics 177 (2006) 377–387.
[48] M.J.L. Ostergard, M. Mogenson, Electrochim. Acta 38 (1993) 2015–2020.
[49] M. Liu, D. Ding, K. Blinn, X. Li, L. Nie, M. Liu, Int. J. Hydrogen Energy 37 (2012) 8613–8620.
[50] J.F. Gao, X.Q. Liu, D.K. Peng, G.Y. Meng, Catal. Today 82 (2003) 207–211.
[51] S.P. Simner, M.D. Anderson, M.H. Engelhard, J.W. Stevenson, Electrochem. Solid State Lett. 9 (2006) A478–A481.
[52] H. Yokokawa, N. Sakai, T. Horita, K. Yamaji, M.E. Brito, H. Kishimoto, J. Alloys Compd. 452 (2008) 41–47.